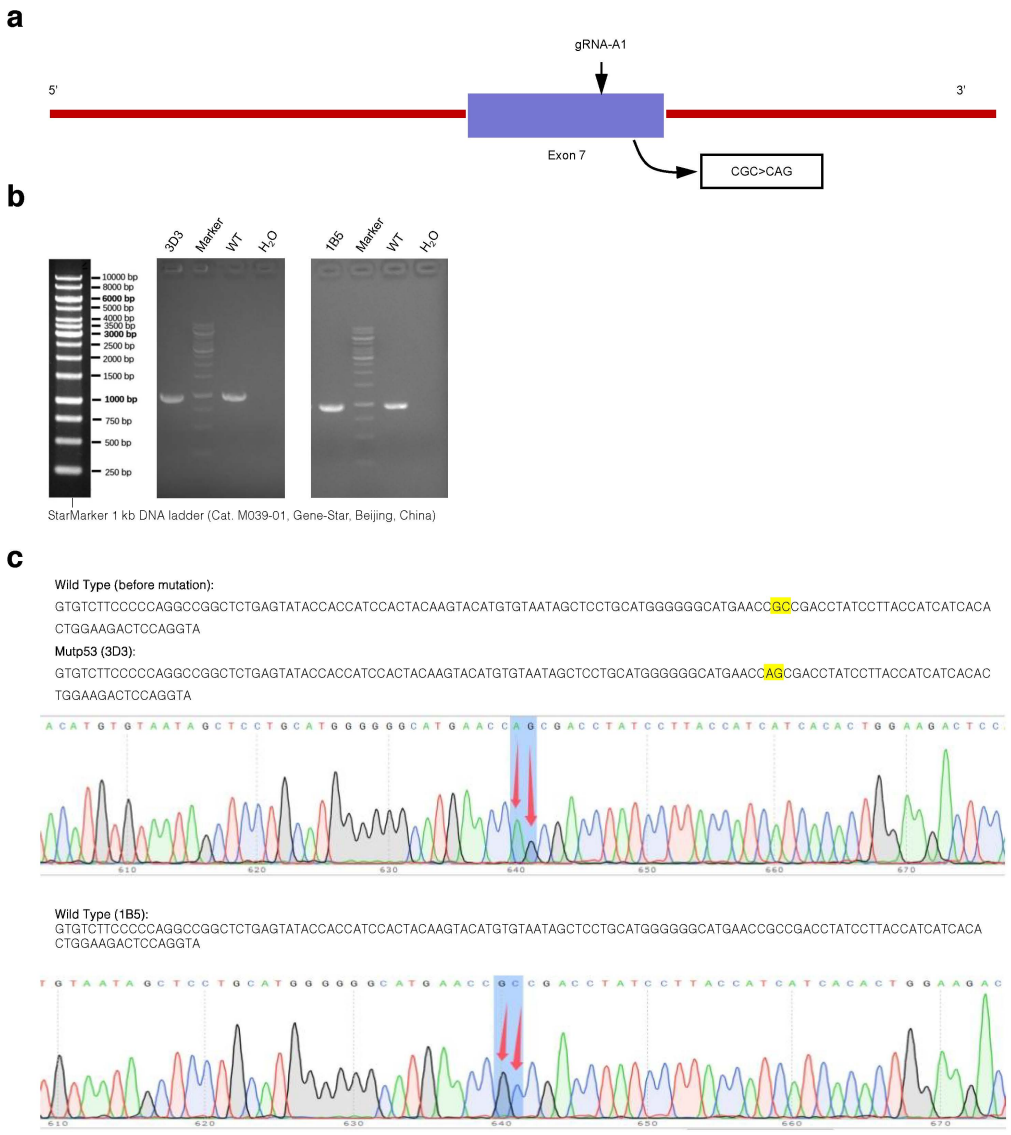

Fig. S1. Design and validation of *TP53* exon 7 point-mutated cell clones in Myc-Cap cell line. (**a**) Schematic diagram showing the gene-editing strategy. A guide RNA (gRNA-A1) targets exon 7 of the *TP53*; the desired base substitution changes the codon CGC to CAG, resulting in an arginine-to-glutamine (Arg→Gln) amino acid change. (**b**) Polymerase chain reaction (PCR) followed by restriction enzyme digestion and analysis via agarose gel electrophoresis. Left: clone 3D3; right: clone 1B5. Each panel includes a DNA size marker (ladder), a wild-type control (WT), and a no-template control (NTC, labeled H_2O). (**c**) Sanger sequencing validation. The upper trace shows the sequence of clone 3D3, demonstrating a homozygous CGC→CAG mutation.

The lower trace shows clone 1B5, which retains the wild-type sequence (CGC), confirming a homozygous WT genotype. The target codons are highlighted in yellow.

Note: Abbreviations: WT, wild type; NTC, no-template control; gRNA, guide RNA; PCR, polymerase chain reaction.

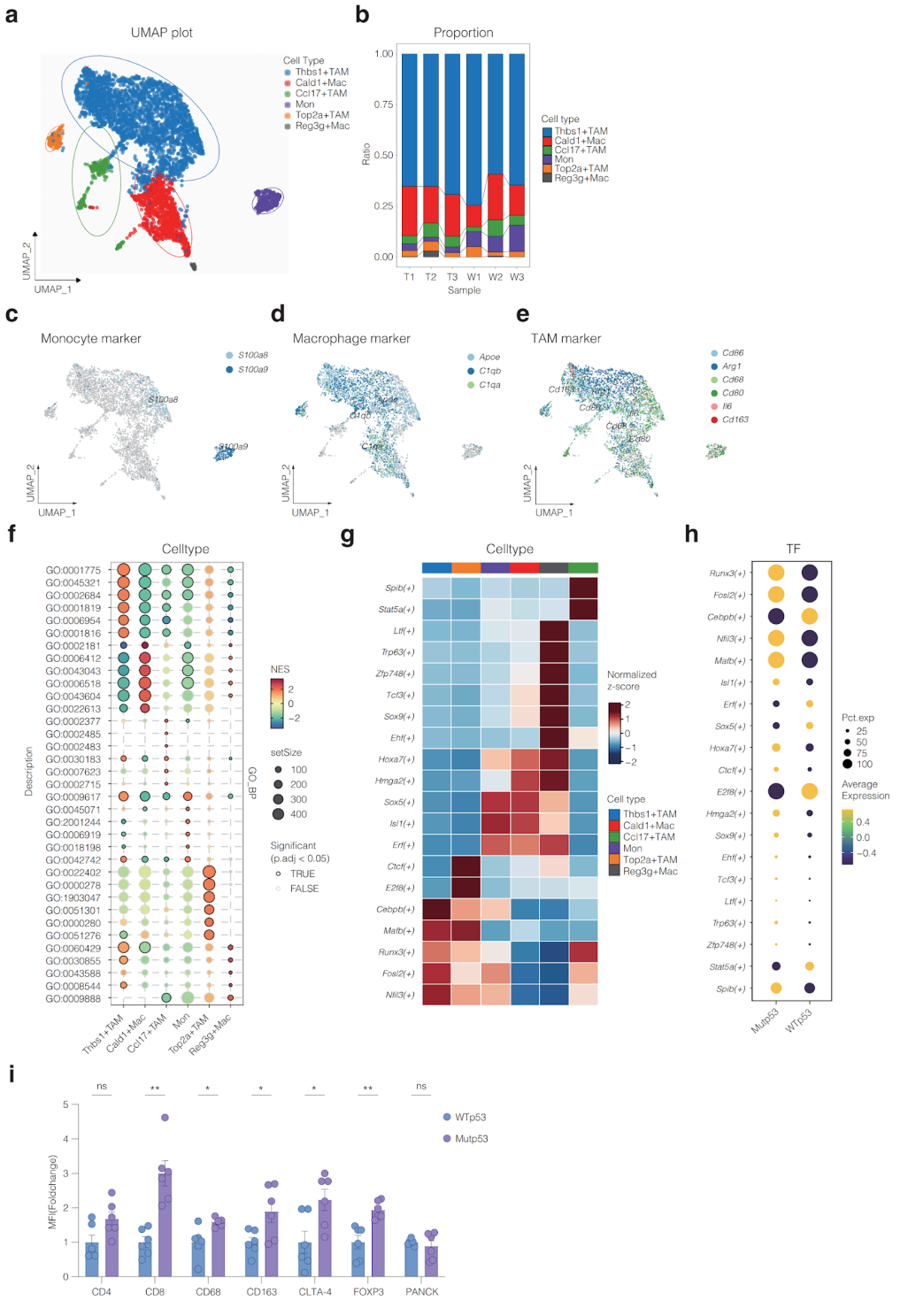

Fig. S2. Single-cell characterization of monocytes and tumor-associated macrophages in mutant p53 tumors versus wild-type tumors. (**a**) UMAP visualization of myeloid cell populations from WTp53 and Mutp53 tumors, showing distinct clusters of monocytes and

macrophages, including tumor-associated macrophages (TAMs). (**b**) Proportion analysis of myeloid subpopulations across individual tumor samples (T1-T3: Mutp53; W1-W3: WTp53). (**c**) Expression of monocyte-specific markers (e.g., *S100a8*, *S100a9*), confirming cluster identity. (**d**) Expression of macrophage-related markers (e.g., *Apoe*, *C1qa*, *C1qb*). (**e**) Expression of TAM-associated markers (*Cd86*, *Arg1*, *Cd163*, and *Il6*). (**f**) Gene Ontology (GO) enrichment analysis of each myeloid subpopulation, with bubble plots representing normalized enrichment scores (NES), gene set size, and statistical significance. (**g**) Transcription factor (TF) activity analysis across myeloid subpopulations, indicating dominant TFs. (**h**) Differential TF activity between WTp53 and Mutp53 tumors, showing key regulators (*Runx3*, *Fosl2*, *Nfil3*, *Mafb*) that distinguish mutant versus wild-type states. (**j**) Multiplex immunofluorescence quantification of immune infiltration.

Note: Abbreviations: UMAP, uniform manifold approximation and projection; TAM, tumor-associated macrophage; GO, Gene Ontology; TF, transcription factor; Mutp53, mutant p53; WTp53, wild-type p53.

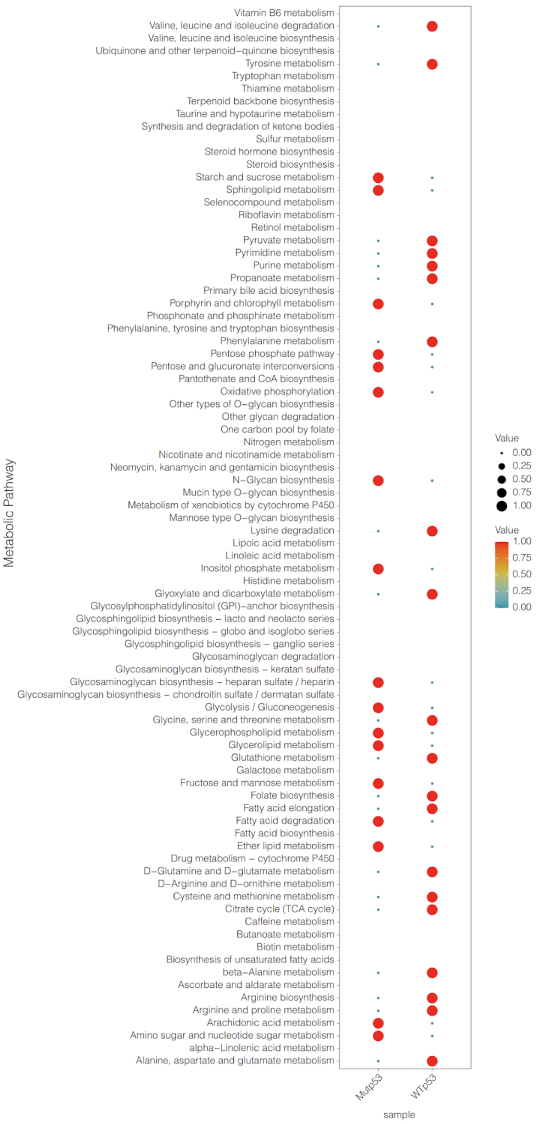

Fig. S3. Single-cell metabolic pathway analysis of epithelial cells in mutant versus wild-type TP53 tumors. Bubble plot depicting the differential activity of metabolic pathways in epithelial cells from the mutant TP53 (Mutp53) and wild-type TP53 (WTp53) groups, analyzed via the scMetabolism package. Each row represents a metabolic pathway, and the columns indicate sample groups. Bubble size indicates pathway enrichment scores; color represents relative metabolic activity (blue = low, red = high). Compared with WTp53 epithelial cells, Mutp53 epithelial cells exhibit distinct metabolic profiles.

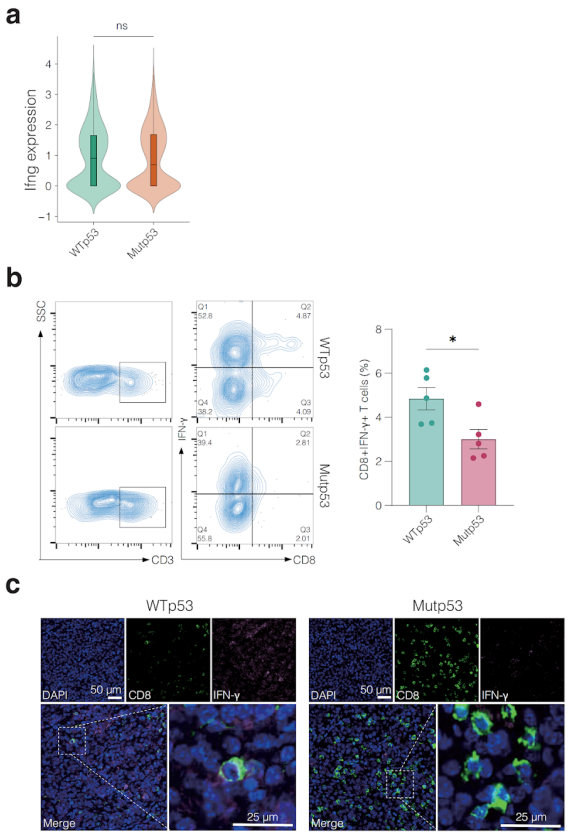

Fig. S4. Mutant p53 reduces interferon-γ-producing CD8+ T cells while enhancing CXCL10 secretion in RM-1 cells. (**a**) Violin plots showing Ifng (interferon gamma) expression in CD8+ T cells from wild-type (WTp53) and mutant p53 (Mutp53) tumors. The centerlines and boxes indicate the median and interquartile range (IQR), respectively. No significant difference was observed (ns, unpaired two-tailed Student's t test). (**b**) Flow cytometry analysis of tumor-infiltrating lymphocytes. Each dot represents a biological replicate (n = 5 tumors/group). The data are shown as the means ± standard errors of the means (SEMs). $p < 0.05$ according to the unpaired two-tailed Student's t test. (**c**) Immunofluorescence staining of tumor sections for DAPI (nuclei, blue), CD8 (green), and IFN-γ (magenta). Merged images showing fewer CD8+ IFN-γ+ cells in Mutp53 tumors. Scale bars, 100 μm. (**d**) CXCL10 levels in the cellular supernatant of RM-1 cells harboring wild-type p53 (WTp53) or mutant p53 (Mutp53) were quantified by ELISA.

Note: Abbreviations: IFN-γ, interferon gamma; IQR, interquartile range; DAPI, 4′,6-diamidino-2-phenylindole.

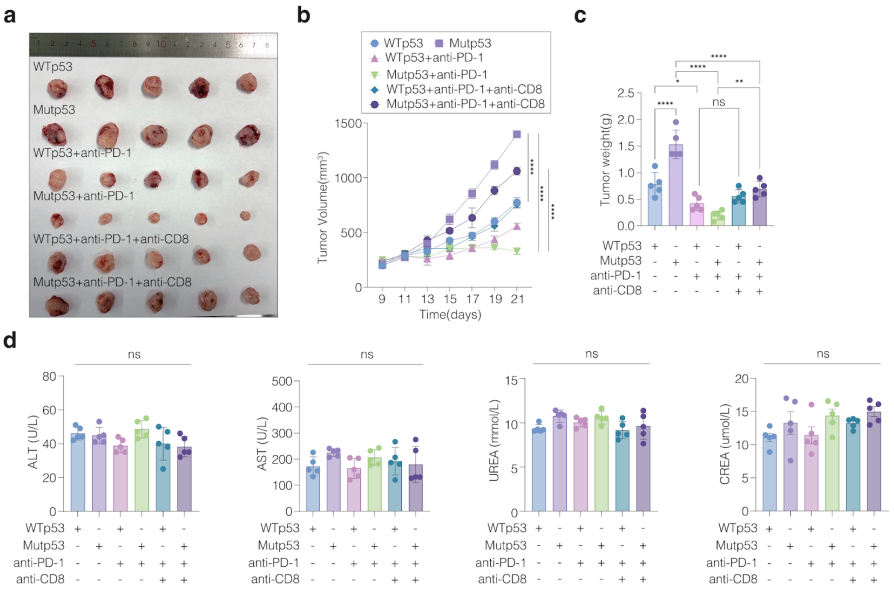

Fig. S5. CD8+ T-cell depletion abrogates the therapeutic efficacy of PD-1 blockade, particularly in Mutp53 tumors, without inducing systemic toxicity. (**a**) Representative images of tumors harvested from mice bearing subcutaneous RM-1 tumors established by injection of 1 × 10^6 WTp53 or Mutp53 cells under the indicated treatment conditions: WTp53, Mutp53, WTp53 + anti-PD-1, Mutp53 + anti-PD-1, WTp53 + anti-PD-1 + anti-CD8, and Mutp53 + anti-PD-1 + anti-CD8. (**b**) Tumor growth curves showing longitudinal changes in tumor volume for each treatment group. CD8+ T-cell depletion markedly attenuated the tumor-suppressive effect of PD-1 blockade, with a more pronounced reversal observed in Mutp53 tumors compared with WTp53 tumors. (**c**) Tumor weights measured at the experimental endpoint. Consistent with tumor growth curves, anti-CD8 treatment significantly restored tumor burden in anti-PD-1-treated mice, particularly in the Mutp53 group. (**d**) Assessment of systemic toxicity following anti-CD8 treatment. Serum levels of alanine aminotransferase (ALT), aspartate aminotransferase (AST), urea, and creatinine (Cre) were measured, revealing no significant differences among treatment groups, indicating minimal impact on liver and kidney function.

Note: Data are presented as the mean±SD. Statistical significance was assessed using one-way or two-way ANOVA with Tukey's multiple-comparison test, as appropriate. $p < 0.05$, $p < 0.01$, *$p < 0.001$; ns, not significant.

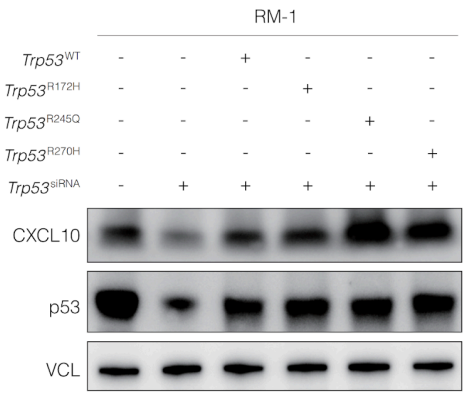

Fig. S6. CXCL10 expression following *Trp53* knockdown and re-expression of *Trp53* variants.

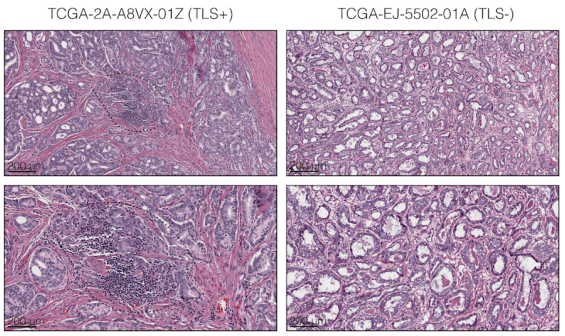

Fig. S7. Representative H&E images from TCGA prostate cancer samples. Representative hematoxylin and eosin (H&E)-stained sections from TCGA prostate cancer cases. Left, a tumor sample with intratumoral tertiary lymphoid structures (TLS-positive) and *TP53* mutation; right, a tumor sample without detectable TLS and without *TP53* mutation. Images are shown at 20× and 40× magnification.

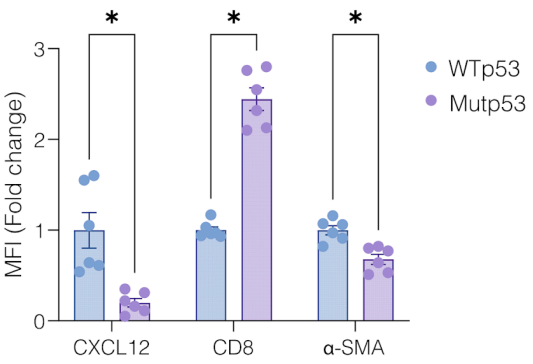

Fig. S8. Quantification of mean fluorescence intensity (MFI) for CXCL12, CD8, and α-SMA in WTp53 and Mutp53 tumors corresponding to Fig. 6g.